# A new uranyl oxide hydrate sheet in vandendriesscheite: Implications for mineral paragenesis and the corrosion of spent nuclear fuel

## Peter C. Burns*

Department of Geology, University of Illinois at Urbana-Champaign, 245 Natural History Building,
1301 West Green Street, Urbana, Illinois 61801, U.S.A.

## Abstract

The structure of vandendriesscheite, $Z = 8$, $Pb_{1.57}[(UO_2)_{10}O_6(OH)_{11}](H_2O)_{11}$, orthorhombic, $a = 14.1165(6)$, $b = 41.378(2)$, $c = 14.5347(6)$ Å, $V = 8490$ Å$^3$, space group $Pbca$, has been solved by direct methods and refined by full-matrix least-squares techniques to an agreement factor ($R$) of 12.1% and a goodness-of-fit ($S$) of 1.28 using 4918 unique observed reflections ($|F_o| \geq 4\sigma F$) collected with Mo$K\alpha$ X-radiation and a CCD (charge-coupled device) detector. The structure contains ten unique U$^{6+}$ positions, each of which is part of a nearly linear $(UO_2)^{2+}$ uranyl ion that is further coordinated by five equatorial $(O^{2-}, OH^-)$ anions to form pentagonal bipyramidal polyhedra. There are two unique Pb positions; one is fully occupied, but site-scattering refinement gives an occupancy factor of 0.573(8) for the other. The Pb positions are coordinated by O atoms of the uranyl ions and by $H_2O$ groups. There are 11 unique $H_2O$ groups; five are bonded to Pb and the other six are held in the structure by hydrogen bonds only. The U polyhedra link by the sharing of equatorial edges to form sheets parallel to (001). The sheet of U polyhedra is not known from another structure and is the most complex yet observed in a uranyl oxide hydrate. The sheets are structurally intermediate to those in schoepite and becquerelite and are linked by bonds to the interlayer Pb cations and the $H_2O$ groups. The extensive network of hydrogen bonds that link adjacent sheets is derived on the basis of crystal-chemical constraints.

The high mobility of U$^{6+}$ in oxidizing fluids, as opposed to Pb$^{2+}$, causes the alteration products of Precambrian uraninite deposits to become progressively enriched in Pb relative to U. In the case of lead uranyl oxide hydrate minerals, there is a continuous sequence of crystal structures that involves a systematic modification of the sheets of U polyhedra and that corresponds to increasing sheet charge and increasing Pb content. Thus, a clear relationship exists between the crystal structures of lead uranyl oxide hydrates and their paragenesis, and this is relevant to the disposal of spent nuclear fuel.

## Introduction

Uranyl minerals are major constituents of the oxidized portion of U deposits, where they occur most commonly as the products of alteration of uraninite (Frondel 1958; Finch and Ewing 1992; Pearcy et al. 1994). Recently these minerals have received a renewed interest because of their significance to the environment. Uranyl minerals are products of the oxidation of U mine tailings and they impact upon the release rates of U and Pb. Furthermore, uranyl minerals are prominent alteration phases in laboratory experiments on UO$_2$ as well as spent nuclear fuel subjected to oxidative dissolution (Wadsten 1977; Wang and Katayama 1982; Wronkiewicz et al. 1992, 1996; Forsyth and Werme 1992; Johnson and Werme 1994; Finn et al. 1996). The details of the occurrence of uranyl minerals thus place important constraints on the extrapolation of the results of short-term experiments to periods relevant to nuclear-waste disposal (Ewing 1993). Despite their importance, uranyl minerals are often poorly characterized and in general systematic work on the structures and stabilities of these minerals is lacking.

An understanding of the relationship between the crystal structures of uranyl minerals and their paragenesis is fundamental to studies of the alteration of U deposits, U mine tailings, and the UO$_2$ in spent nuclear fuel. Toward this goal, Burns et al. (1996) provided a hierarchy of structures and comparison of 180 uranyl minerals and synthetic inorganic phases. Crystal-structure studies of uranyl minerals are often made intractable by the poor quality of the crystals and severe absorption effects. As a result, the structures are known and refined for only about 30% of described uranyl minerals, despite the considerable effort expended by several research groups. This contribution reports the first determination of the structure of the uranyl mineral vandendriesscheite.

* Current address: Department of Civil Engineering and Geological Sciences, University of Notre Dame, Notre Dame, IN 46556-0767.

**TABLE 1.** Crystallographic data for vandendriesscheite

| | | | |
|---|---|---|---|
| $a$ (Å) | 14.1165(6) | Crystal size (mm) | $0.16 \times 0.10 \times 0.045$ |
| $b$ (Å) | 41.378(2) | Radiation | Mo$K\alpha$ |
| $c$ (Å) | 14.5347(6) | Total Ref. | 53227 |
| $V$ (Å³) | 8490(1) | Unique Ref. | 10257 |
| | | Unique $|F_o| \geq 4\sigma_F$ | 4918 |
| Space group | $Pbca$ | Final $R^*$ | 12.1 |
| $F_{000}$ | 11726 | Final $S$† | 1.28 |
| $\mu$ (cm⁻¹) | 443.2 | $D_{calc}$ (g/cm³) | 5.487 |

Unit-cell contents: $8\{Pb_{1.57}[(UO_2)_{10}O_6(OH)_{11}])(H_2O)_{11}$

\* $R = \Sigma(|F_o| - |F_c|)/\Sigma|F_o|$.
† $S = [\Sigma w(|F_o| - |F_c|)^2/(m - n)]^{1/2}$, for $m$ observations and $n$ parameters.

## PREVIOUS STUDIES

Vandendriesscheite, a lead uranyl oxide hydrate, is quite common in the oxidized portions of Precambrian U deposits. It was first described from Shinkolobwe (Congo) by Vaes (1947). Protas (1959) examined several crystals of vandendriesscheite and obtained various unit cells. He also reported that a range of compositions might occur and gave the formulae $0.97PbO\cdot7UO_3\cdot12.5H_2O$ and $1.06PbO\cdot6UO_3\cdot8.1H_2O$ for two samples. Christ and Clark (1960) examined crystals from a single specimen from the Shinkolobwe (Congo) deposit and observed that most crystals contained two phases, designated vandendriesscheite I and II. They demonstrated that dehydration of vandendriesscheite I can result in vandendriesscheite II. The crystals examined contained either vandendriesscheite I or II dominantly, with only minor amounts of the other phase present. Christ and Clark (1960) gave similar unit-cell dimensions for each phase, with both the $b$ and $c$ dimensions longer than 40 Å. The reflections requiring $b \approx 41$ Å were sharp and numerous, whereas reflections that required $c \approx 43$ Å were reported to be very faint, diffuse, and relatively sparse. Pagoaga (1983) obtained chemical analyses using an electron microprobe for crystals of vandendriesscheite (NMNH 149661) from an unspecified locality. These analyses gave the formula $1.1PbO\cdot7UO_3\cdot6.4H_2O$.

## EXPERIMENTAL METHODS

Single-crystal diffraction studies of vandendriesscheite are difficult because of the small size of the crystals and the long unit-cell lengths that cause serious overlap problems for data collected on conventional four-circle diffractometers. For these reasons, the structure of vandendriesscheite remained unknown. The sample of vandendriesscheite studied is from Shinkolobwe (Congo) and is housed under the sample identification UNM654 in the Department of Earth and Planetary Sciences, University of New Mexico. The sample consists of uraninite with a ~0.5 cm thick corrosion rind of yellow and orange uranyl minerals. A small tabular crystal (flattened on {001}) of vandendriesscheite was selected for data collection following the optical examination of several dozen crystals. The crystal selected showed sharp extinction between crossed polarizers and was free of inclusions.

The crystal was mounted on a Siemens three-circle dif-

fractometer equipped with a SMART CCD (charge-coupled device) detector with a crystal-to-detector distance of 5 cm. The SMART CCD detector is a two-dimensional area detector with a 9 cm input imaging area. The detector uses a phosphor screen, located immediately behind a beryllium window, to convert the X-ray photons to optical photons that are carried through a fiber-optic taper to the CCD chip. This detector provides much improved resolution, sensitivity to low-intensity reflections, and shorter data collection time in comparision with a conventional four-circle diffractometer with a scintillation detector. The data were collected using monochromated Mo$K\alpha$ X-radiation and the $\omega$ scan mode with steps of $\omega$ of 0.2°. Note that data collection with the SMART CCD system is independent of the unit-cell dimensions; a full three-dimensional hemisphere of data was collected. The data were then analyzed to locate peaks for unit-cell dimension refinement. The unit-cell dimensions (Table 1) were refined from 5627 reflections using least-squares techniques. The unit-cell dimensions obtained in this study are similar to those reported by Protas (1959): $a = 14.05(5)$, $b = 41.40(5)$, $c = 14.68(5)$; the three-dimensional data set contained no reflections that indicated a larger unit cell, such as reported by Christ and Clark (1960). The hemisphere of data was collected for $3° \leq 2\theta \leq 56.5°$ in roughly 6 h, and examination of the intensities of standard reflections showed that the crystal was stable during data collection. The three-dimensional data set was reduced and filtered for statistical outliers using the Siemens program SAINT. The data was corrected for Lorentz, polarization and background effects. A Gaussian absorption correction was performed for $\mu = 443.2$ cm⁻¹ on the basis of measurements and indices of the crystal faces using the Siemens program XPREP. A total of 53 227 reflections were collected, of which there were 10 257 unique reflections with 4918 classed as observed ($|F_o| \geq 4\sigma F$).

## STRUCTURE SOLUTION AND REFINEMENT

Scattering curves for neutral atoms, together with anomalous dispersion corrections, were taken from Cromer and Mann (1968) and Cromer and Liberman (1970), respectively. The Siemens SHELXTL Version 5 system of programs was used.

Reflection statistics indicated that the space groups

**TABLE 2.** Atomic coordinates and equivalent isotropic displacement factors for vandendriesscheite

|        | $x$        | $y$         | $z$       | $U_{eq}$  |
|--------|------------|-------------|-----------|-----------|
| U1     | 0.7236(1)  | 0.15997(4)  | 0.7251(1) | 123(4)    |
| U2     | 0.5075(1)  | 0.10404(4)  | 0.7649(1) | 140(4)    |
| U3     | 1.0041(1)  | 0.39961(4)  | 0.7661(1) | 125(4)    |
| U4     | 0.9715(1)  | 0.19612(4)  | 0.7467(1) | 115(4)    |
| U5     | 0.7354(1)  | 0.45539(4)  | 0.7543(1) | 128(4)    |
| U6     | 0.9709(1)  | 0.30853(4)  | 0.7495(1) | 119(4)    |
| U7     | 0.7561(1)  | 0.25228(4)  | 0.7544(1) | 112(4)    |
| U8     | 0.7275(1)  | 0.04795(4)  | 0.7442(1) | 141(4)    |
| U9     | 1.2235(1)  | 0.34481(4)  | 0.7351(1) | 138(4)    |
| U10    | 0.9845(1)  | 0.00867(4)  | 0.7264(1) | 171(4)    |
| Pb1    | 0.8112(1)  | 0.30459(5)  | 0.4976(1) | 262(5)    |
| Pb2    | 0.8903(5)  | −0.0004(1)  | 1.0020(4) | 745(24)   |
| O1     | 0.817(2)   | 0.2040(12)  | 0.726(2)  | 130(63)   |
| OH2    | 0.627(2)   | 0.2162(7)   | 0.713(2)  | 139(65)   |
| O3     | 0.746(2)   | 0.1577(8)   | 0.845(2)  | 195(73)   |
| OH4    | 0.386(2)   | 0.1440(7)   | 0.802(2)  | 119(64)   |
| O5     | 0.705(2)   | 0.1635(7)   | 0.603(2)  | 131(65)   |
| OH6    | 0.682(2)   | 0.1037(7)   | 0.704(2)  | 176(69)   |
| O7     | 0.569(2)   | 0.1545(8)   | 0.756(2)  | 185(71)   |
| OH8    | 0.379(2)   | 0.0680(8)   | 0.803(2)  | 267(83)   |
| O9     | 0.539(2)   | 0.1039(9)   | 0.885(2)  | 346(91)   |
| O10    | 0.569(2)   | 0.0523(8)   | 0.754(2)  | 208(74)   |
| O11    | 0.472(2)   | 0.1037(8)   | 0.648(2)  | 281(83)   |
| OH12   | 1.188(2)   | 0.3999(7)   | 0.784(2)  | 155(65)   |
| O13    | 1.000(2)   | 0.4125(8)   | 0.654(2)  | 259(80)   |
| O14    | 1.066(2)   | 0.3513(7)   | 0.721(2)  | 87(59)    |
| OH15   | 0.879(2)   | 0.3637(8)   | 0.734(2)  | 265(81)   |
| O16    | 1.012(2)   | 0.3887(8)   | 0.885(2)  | 210(74)   |
| OH17   | 0.932(2)   | −0.0470(7)  | 0.700(2)  | 106(62)   |
| OH18   | 0.865(2)   | 0.4273(7)   | 0.811(2)  | 179(73)   |
| OH19   | 0.938(2)   | 0.2532(7)   | 0.783(2)  | 120(62)   |
| O20    | 0.947(2)   | 0.1865(8)   | 0.863(2)  | 215(75)   |
| O21    | 0.995(2)   | 0.2071(8)   | 0.626(2)  | 239(78)   |
| OH22   | 1.149(2)   | −0.0031(7)  | 0.696(2)  | 89(60)    |
| O23    | 0.690(2)   | 0.4522(7)   | 0.869(2)  | 110(63)   |
| O24    | 0.833(2)   | 0.0057(9)   | 0.752(3)  | 390(98)   |
| O25    | 0.776(2)   | 0.4577(8)   | 0.640(2)  | 287(86)   |
| O26    | 0.814(2)   | 0.3015(7)   | 0.783(2)  | 29(51)    |
| OH27   | 0.628(2)   | 0.2883(8)   | 0.788(2)  | 260(81)   |
| O28    | 0.939(2)   | 0.3032(7)   | 0.628(2)  | 115(62)   |
| O29    | 0.999(2)   | 0.3132(8)   | 0.868(2)  | 251(80)   |
| O30    | 0.763(2)   | 0.2643(9)   | 0.636(2)  | 263(81)   |
| O31    | 0.748(2)   | 0.2403(9)   | 0.873(2)  | 269(79)   |
| O32    | 0.707(2)   | 0.0364(9)   | 0.624(2)  | 304(86)   |
| O33    | 0.751(2)   | 0.0604(8)   | 0.860(2)  | 261(81)   |
| O34    | 1.218(2)   | 0.3355(7)   | 0.858(2)  | 136(65)   |
| O35    | 1.229(2)   | 0.3549(9)   | 0.613(2)  | 314(88)   |
| O36    | 0.968(2)   | 0.0131(8)   | 0.607(2)  | 205(73)   |
| O37    | 1.002(3)   | −0.0004(9)  | 0.850(3)  | 491(111)  |
| H$_2$O38 | 0.353(3) | 0.0757(9)   | 0.993(3)  | 438(106)  |
| H$_2$O39 | 1.073(2) | 0.4484(9)   | 0.980(2)  | 269(87)   |
| H$_2$O40 | 0.386(3) | 0.146(1)    | 0.981(3)  | 512(121)  |
| H$_2$O41 | 0.634(4) | 0.319(1)    | 0.481(4)  | 1017(202) |
| H$_2$O42 | 0.627(2) | 0.2146(9)   | 0.504(3)  | 357(91)   |
| H$_2$O43 | 0.713(2) | 0.3954(9)   | 0.513(2)  | 348(96)   |
| H$_2$O44 | 0.945(3) | 0.256(1)    | 0.478(3)  | 468(115)  |
| H$_2$O45 | 0.155(3) | 0.098(1)    | 0.981(3)  | 554(128)  |
| H$_2$O46 | 1.006(5) | −0.051(2)   | 1.007(6)  | 1498(307) |
| H$_2$O47 | 0.875(3) | 0.363(1)    | 0.528(3)  | 427(104)  |
| H$_2$O48 | 0.692(3) | −0.001(1)   | 0.975(3)  | 548(128)  |

*Note:* $U_{eq} = U_{eq} \times 10^4$.

**TABLE 3.** Anisotropic displacement parameters for cations in the structure of vandendriesscheite

|      | $U_{11}$  | $U_{22}$  | $U_{33}$  | $U_{12}$  | $U_{13}$  | $U_{23}$  |
|------|-----------|-----------|-----------|-----------|-----------|-----------|
| U1   | 110(8)    | 96(9)     | 164(8)    | −10(6)    | −14(7)    | 8(7)      |
| U2   | 106(8)    | 81(9)     | 233(9)    | 2(6)      | 19(7)     | 11(7)     |
| U3   | 125(8)    | 94(9)     | 155(8)    | 14(7)     | −6(7)     | −5(6)     |
| U4   | 94(7)     | 79(9)     | 173(8)    | 7(6)      | 15(6)     | 0(7)      |
| U5   | 99(8)     | 72(9)     | 212(9)    | −11(6)    | 7(7)      | 0(7)      |
| U6   | 108(7)    | 80(9)     | 169(8)    | 0(6)      | −7(6)     | −3(6)     |
| U7   | 105(7)    | 67(9)     | 162(7)    | 7(6)      | 15(7)     | 8(6)      |
| U8   | 109(8)    | 69(9)     | 245(9)    | −10(7)    | 15(7)     | 6(6)      |
| U9   | 135(8)    | 115(9)    | 166(9)    | −6(7)     | 0(7)      | 48(6)     |
| U10  | 168(8)    | 135(9)    | 210(8)    | −32(7)    | 27(7)     | −58(7)    |
| Pb1  | 299(9)    | 250(12)   | 237(9)    | −13(9)    | −13(9)    | −34(9)    |
| Pb2  | 1510(61)  | 391(35)   | 336(23)   | 7(19)     | 42(32)    | −131(33)  |

*Note:* All $U$ values multiplied by $10^4$.

finement of all atomic positional parameters, allowing for isotropic atomic-displacement, provided a model with an agreement factor ($R$) of 13.9%. Conversion of the displacement parameters for the Pb and U atoms to anisotropic, together with refinement of the positional parameters for all atoms and the isotropic-displacement parameters for the anion positions, gave an agreement index ($R$) of 12.1% for observed relections ($|F_o| \geq 4\sigma F$) and a goodness-of-fit ($S$) of 1.27. Both an isotropic extinction correction and a refinable structure-factor weighting scheme were tried, but neither improved the refinement. In the final cycle of refinement the average parameter shift/esd was 0.000 and the maximum was 0.008, which corresponded to a shift of 0.001 Å of the H$_2$O46 position. The maximum and minimum peaks in the final difference-Fourier maps were 4.0 and −4.4 e/Å$^3$, respectively. Final positional and displacement parameters, cation anisotropic-displacement parameters, calculated and observed structure factors, selected interatomic distances, and bond-valence sums at the cation and anion positions are presented in Tables 2–6[1], respectively.

## RESULTS

### Formula of vandendriesscheite

The structure solution indicates that there are ten symmetrically distinct U positions; bond-valence sums (Table 6) show these to correspond to U$^{6+}$. There are two symmetrically distinct Pb sites; one is fully occupied and the other has a refined occupancy factor of 0.573(8). A total of 48 symmetrically distinct anion positions occur in the structure; the bond-valence analysis (Table 6) indicates that these correspond to 26 O atoms, 11 OH$^-$ groups, and 11 H$_2$O groups. All atoms are on general positions in the space group *Pbca*; thus the structural formula for the crystal studied is Pb$_{1.57}$[(UO$_2$)$_{10}$O$_6$(OH)$_{11}$](H$_2$O)$_{11}$, $Z = 8$. The calculated density of 5.487 g/cm$^3$ compares favorably

*Pbca* or *P2$_1$ca* were the most likely. Successful solution and refinement of the structure was achieved in the space group *Pbca*. The structure was solved by direct methods; the resulting model contained the positions of the U and Pb atoms, as well as some of the anions. Additional anion positions were located on difference-Fourier maps calculated after least-squares refinement of the model. Re-

**TABLE 5.** Selected interatomic distances and bond angles in the structure of vandendriesscheite

| | | | |
|---|---|---|---|
| U1-O3 | 1.78(3) | U2-O11 | 1.78(3) |
| U1-O5 | 1.80(3) | U2-O9 | 1.79(4) |
| U1-O7 | 2.24(3) | U2-O7 | 2.27(3) |
| U1-O1 | 2.25(3) | U2-O10 | 2.32(3) |
| U1-OH6 | 2.42(3) | U2-OH8 | 2.42(3) |
| U1-OH4a | 2.42(3) | U2-OH4 | 2.44(3) |
| U1-OH2 | 2.70(3) | U2-OH6 | 2.62(3) |
| $\langle$U1-O$_{Ur}\rangle$ | 1.79 | $\langle$U2-O$_{Ur}\rangle$ | 1.78 |
| O$_{Ur}$-U1-O$_{Ur}$ | 178(1) | O$_{Ur}$-U2-O$_{Ur}$ | 178(1) |
| $\langle$U1-$\phi_{eq}\rangle$ | 2.41 | $\langle$U2-$\phi_{eq}\rangle$ | 2.41 |
| U3-O13 | 1.71(3) | U4-O20 | 1.77(3) |
| U3-O16 | 1.79(3) | U4-O21 | 1.85(3) |
| U3-O14 | 2.27(3) | U4-O7a | 2.21(3) |
| U3-OH15 | 2.36(3) | U4-O1 | 2.23(3) |
| U3-OH18 | 2.37(3) | U4-OH2a | 2.42(3) |
| U3-OH17b | 2.44(3) | U4-OH19 | 2.46(3) |
| U3-OH12 | 2.61(3) | U4-OH4a | 2.57(3) |
| $\langle$U3-O$_{Ur}\rangle$ | 1.75 | $\langle$U4-O$_{Ur}\rangle$ | 1.81 |
| O$_{Ur}$-U3-O$_{Ur}$ | 176(1) | O$_{Ur}$-U4-O$_{Ur}$ | 179(1) |
| $\langle$U3-$\phi_{eq}\rangle$ | 2.41 | $\langle$U4-$\phi_{eq}\rangle$ | 2.38 |
| U5-O25 | 1.76(3) | U6-O29 | 1.78(3) |
| U5-O23 | 1.79(3) | U6-O28 | 1.84(3) |
| U5-O24c | 2.29(4) | U6-O14 | 2.26(3) |
| U5-OH18 | 2.32(3) | U6-O26 | 2.28(2) |
| U5-OH12d | 2.46(3) | U6-O19 | 2.39(3) |
| U5-OH22b | 2.48(3) | U6-OH27a | 2.43(3) |
| U5-OH17c | 2.49(3) | U6-OH15 | 2.64(3) |
| $\langle$U5-O$_{Ur}\rangle$ | 1.77 | $\langle$U6-O$_{Ur}\rangle$ | 1.81 |
| O$_{Ur}$-U5-O$_{Ur}$ | 178(1) | O$_{Ur}$-U6-O$_{Ur}$ | 179(1) |
| $\langle$U5-$\phi_{eq}\rangle$ | 2.41 | $\langle$U6-$\phi_{eq}\rangle$ | 2.40 |
| U7-O30 | 1.79(3) | U8-O33 | 1.79(3) |
| U7-O31 | 1.80(3) | U8-O32 | 1.83(3) |
| U7-O1 | 2.21(3) | U8-O10 | 2.25(3) |
| U7-O26 | 2.23(3) | U8-O24 | 2.29(4) |
| U7-OH27 | 2.40(3) | U8-OH8a | 2.39(3) |
| U7-OH2 | 2.43(3) | U8-OH6 | 2.47(3) |
| U7-OH19 | 2.60(3) | U8-OH22d | 2.54(3) |
| $\langle$U7-O$_{Ur}\rangle$ | 1.79 | $\langle$U8-O$_{Ur}\rangle$ | 1.81 |
| O$_{Ur}$-U7-O$_{Ur}$ | 179(1) | O$_{Ur}$-U8-O$_{Ur}$ | 177(2) |
| $\langle$U7-$\phi_{eq}\rangle$ | 2.37 | $\langle$U8-$\phi_{eq}\rangle$ | 2.39 |
| U9-O35 | 1.82(3) | U10-O36 | 1.76(3) |
| U9-O34 | 1.83(3) | U10-O37 | 1.85(4) |
| U9-O26a | 2.22(3) | U10-O24 | 2.18(3) |
| U9-O14 | 2.26(2) | U10-O10a | 2.18(3) |
| U9-OH15a | 2.37(3) | U10-OH22 | 2.41(2) |
| U9-OH12 | 2.44(3) | U10-OH17 | 2.45(3) |
| U9-OH27a | 2.72(3) | U10-OH8a | 2.91(3) |
| $\langle$U9-O$_{Ur}\rangle$ | 1.82 | $\langle$U10-O$_{Ur}\rangle$ | 1.80 |
| O$_{Ur}$-U9-O$_{Ur}$ | 179(1) | O$_{Ur}$-U10-O$_{Ur}$ | 174(2) |
| $\langle$U9-$\phi_{eq}\rangle$ | 2.40 | $\langle$U10-$\phi_{eq}\rangle$ | 2.43 |
| Pb1-H$_2$O41 | 2.58(6) | Pb2-H$_2$O46f | 2.58(8) |
| Pb1-O28 | 2.62(3) | Pb2-O37f | 2.63(4) |
| Pb1-H$_2$O47 | 2.62(4) | Pb2-H$_2$O46 | 2.64(8) |
| Pb1-O30 | 2.71(3) | Pb2-O32g | 2.69(4) |
| Pb1-O31e | 2.74(3) | Pb2-O37 | 2.71(4) |
| Pb1-O20e | 2.76(3) | Pb2-H$_2$O48 | 2.83(4) |
| Pb1-H$_2$O44 | 2.77(3) | Pb2-O23h | 2.98(4) |
| Pb1-O34d | 2.79(3) | Pb2-O25I | 3.12(4) |
| Pb1-O3e | 2.86(3) | $\langle$Pb2-$\phi\rangle$ | 2.77 |
| $\langle$Pb1-$\phi\rangle$ | 2.72 | | |

*Note:* a = $x + \frac{1}{2}$, $y$, $-z + 1\frac{1}{2}$; b = $-x + 2$, $y + \frac{1}{2}$, $-z + 1\frac{1}{2}$; c = $-x + 1\frac{1}{2}$, $y + \frac{1}{2}$, $z$; d = $x - \frac{1}{2}$, $y$, $-z + 1\frac{1}{2}$; e = $x$, $-y + \frac{1}{2}$, $z - \frac{1}{2}$; f = $-x + 2$, $-y$, $-z + 2$; g = $-x + 1\frac{1}{2}$, $-y$, $z + \frac{1}{2}$; h = $x - 1$, $y + \frac{1}{2}$, $-z + \frac{1}{2}$; i = $x$, $-y + \frac{1}{2}$; $z + \frac{1}{2}$.

with the measured densities 5.45 g/cm$^3$ (Christ and Clark 1960) and 5.46 g/cm$^3$ (Frondel 1958). The formula, rewritten as $1.10PbO \cdot 7UO_3 \cdot 11.55H_2O$, is similar to the formula $0.97PbO \cdot 7UO_3 \cdot 12.5H_2O$ reported by Protas (1959). It contains much more $H_2O$ than the formula

$1.1PbO \cdot 7UO_3 \cdot 6.4H_2O$ obtained by Pagoaga (1983), although the Pb:U ratios are in good agreement.

## U polyhedra

The U$^{6+}$ cation is almost invariably present in crystal structures as part of a near-linear (U$^{6+}$O$_2$)$^{2+}$ uranyl ion (Ur) (Evans 1963; Burns et al. 1996, 1997). The uranyl ion is coordinated by four, five, or six additional anions, such that the uranyl-ion O atoms form the apices of square, pentagonal, and hexagonal bipyramids. Of these three coordination polyhedra, the pentagonal bipyramid is the most common (Evans 1963). The structure of vandendriesscheite contains ten symmetrically distinct U positions. The bond-valence analysis (Table 6) indicates that all of the U is present as U$^{6+}$, as further verified by the occurrence of a near-linear uranyl ion with U$^{6+}$-O bond lengths of ~1.8 Å at each U site. All ten U atoms are coordinated by five equatorial anions (O$^{2-}$, OH$^-$), arranged approximately in a plane nearly perpendicular to the uranyl ion, completing pentagonal bipyramidal polyhedra.

The U5 uranyl ion is coordinated by four OH$^-$ groups and one O atom; whereas, the remaining nine uranyl ions are each coordinated by three OH$^-$ groups and two O atoms. The $\langle$U$^{6+}$-O$_{Ur}\rangle$ bond lengths range from 1.75 to 1.82 Å, the uranyl ions are nearly linear, and the $\langle$U$^{6+}$-$\phi_{eq}\rangle$ ($\phi$: O$^{2-}$, OH$^-$) bond lengths range from 2.37 to 2.43 Å (Table 5). These polyhedral geometries are in accord with the average bond lengths for Ur$\phi_5$ polyhedra in well-refined structures: $\langle$U$^{6+}$-O$_{Ur}\rangle$ = 1.79(4), $\langle$U$^{6+}$-$\phi_{eq}\rangle$ = 2.37(9) Å (Burns et al. 1997).

## Pb polyhedra

The structure of vandendriesscheite contains two symmetrically distinct Pb$^{2+}$ cations in irregular coordination polyhedra. The Pb1 site, which site-scattering refinement indicates is fully occupied, is coordinated by nine anions with $\langle$Pb1-$\phi\rangle$ = 2.72 Å; six of these are O atoms and the remaining three are H$_2$O groups. Each of the O atoms that bond to Pb1 are also bonded to U$^{6+}$ as part of uranyl ions. Site-scattering refinement gives an occupancy factor for the Pb2 site of 0.573(8). The Pb2 site is coordinated by eight anions with $\langle$Pb2-$\phi\rangle$ = 2.77 Å; five are O atoms of uranyl ions and three are H$_2$O groups. Symmetrically equivalent pairs of Pb2 sites are separated by only 3.10(1) Å, and the refined occupancy indicates that only one of the two sites is usually occupied on a local scale. A vector connecting Pb2 to the symmetrically equivalent Pb2 site is oriented along [100]. The principal mean-square atomic displacement for the site along [100] is 0.153 Å; whereas, the [010] and [001] directions have displacements of 0.038 and 0.033 Å, respectively. The disorder of the Pb2 site along [100] is due to repulsion between adjacent Pb2 sites when both are occupied on a local scale, as must sometimes be the case because the refined site occupancy is significantly greater than 0.5. The O37 and H$_2$O46 anions are positioned so as to permit bonding to either of the two Pb2 sites on a local scale. In both cases, the

**TABLE 6.** Bond-valence sums for cations and anions in vandendriesscheite

| | | | | | | | | | |
|---|---|---|---|---|---|---|---|---|---|
| U1 | 5.87 | O1 | 2.09 | O13 | 1.92 (2.12) | O25 | 1.81 | O37 | 1.90 |
| U2 | 5.83 | OH2 | 1.22 (2.02) | O14 | 1.96 | O26 | 2.03 | H$_2$O38 | 0.00 (2.00) |
| U3 | 6.06 | O3 | 1.81 | OH15 | 1.38 (2.18) | OH27 | 1.24 (2.04) | H$_2$O39 | 0.00 (2.00) |
| U4 | 5.88 | OH4 | 1.30 (2.10) | O16 | 1.64 (1.84) | O28 | 1.75 | H$_2$O40 | 0.00 (2.00) |
| U5 | 5.90 | O5 | 1.60 (1.80) | OH17 | 1.33 (2.13) | O29 | 1.68 (1.88) | H$_2$O41 | 0.28 (1.88) |
| U6 | 5.96 | OH6 | 1.24 (2.04) | OH18 | 1.12 (1.92) | O30 | 1.86 | H$_2$O42 | 0.00 (2.20) |
| U7 | 5.98 | O7 | 2.06 | OH19 | 1.29 (2.09) | O31 | 1.79 (1.99) | H$_2$O43 | 0.00 (2.00) |
| U8 | 5.79 | OH8 | 1.17 (1.97) | O20 | 1.87 | O32 | 1.72 (1.92) | H$_2$O44 | 0.17 (1.97) |
| U9 | 5.70 | O9 | 1.63 (1.83) | O21 | 1.47 (1.87) | O33 | 1.66 (1.86) | H$_2$O45 | 0.00 (2.00) |
| U10 | 5.86 | O10 | 2.02 | OH22 | 1.30 (2.10) | O34 | 1.68 (1.88) | H$_2$O46 | 0.26 (2.06) |
| Pb1 | 1.81 | O11 | 1.70 (1.90) | O23 | 1.75 (1.95) | O35 | 1.55 (1.95) | H$_2$O47 | 0.25 (2.05) |
| Pb2 | 1.47 | OH12 | 1.24 (2.04) | O24 | 2.00 | O36 | 1.74 (1.94) | H$_2$O48 | 0.14 (1.94) |

*Note:* Values calculated using the parameters for U$^{6+}$ from Burns et al. (1997) and Pb$^{2+}$ from Brese and O'Keeffe (1991). Anion sums exclude contributions from H atoms. Values in parentheses include contributions from the proposed hydrogen bonds and are based on the assumption that the donor bond is 0.8 v.u. and the acceptor bond is 0.2 v.u.

refined isotropic-displacement parameters are much higher than for other anions of the same chemical type, indicating that significant positional disorder of these two anions occurs in response to the local occupancy of the Pb2 site.

The partial occupancy of the Pb2 site is in accord with the variable Pb:U ratios reported for vandendriesscheite (Finch 1994). The interlayer Pb sites in the structure of curite (Taylor et al. 1981) also show partial occupancy; refinement indicated that one site was 94% occupied and the other site was 57% occupied, similar to the situation in the structure of vandendriesscheite.

### Sheets of uranyl polyhedra

Projection of the structure along [100] (Fig. 1) shows that it is dominated by sheets of uranyl polyhedra, as is typical for all of the uranyl oxide hydrates for which structures are known. The uranyl polyhedra link to form sheets that are parallel to (001). Bonding between the sheets is through the Pb positions, located roughly halfway between the sheets, and by hydrogen bonding to interlayer H$_2$O groups (Fig. 1).

The sheet of uranyl polyhedra, which occurs at $z \approx$ 0.25 and 0.75, is shown projected along [001] in Figure 2. The sheet contains only Ur$\phi_5$ pentagonal bipyramids that have the uranyl ion oriented roughly perpendicular to the sheet. The $b$ repeat distance in the sheet is 41.378(2) Å, making this the most complex sheet found so far in a uranyl oxide hydrate mineral.

The sheet anion topology, derived using the procedure of Burns et al. (1996), is shown in Figure 2b. All known anion topologies of sheets in the structures of uranyl minerals and inorganic phases are given in Burns et al. (1996); the anion topology of the sheets in the structure of vandendriesscheite is not known from any other structure. The sheet anion topology can be conveniently de-
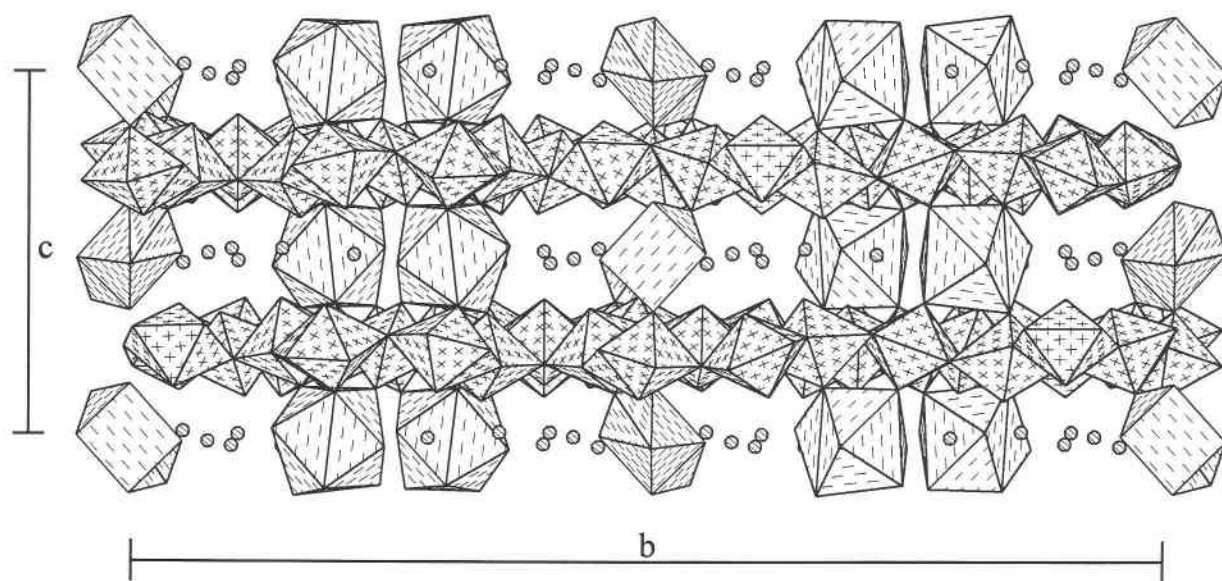


**FIGURE 1.** Polyhedral representation of the structure of vandendriesscheite projected along [100]. The U polyhedra are shaded with crosses, the Pb polyhedra with broken lines, and the H$_2$O groups that are held in the structure by hydrogen bonds only are shown as circles shaded with parallel lines.
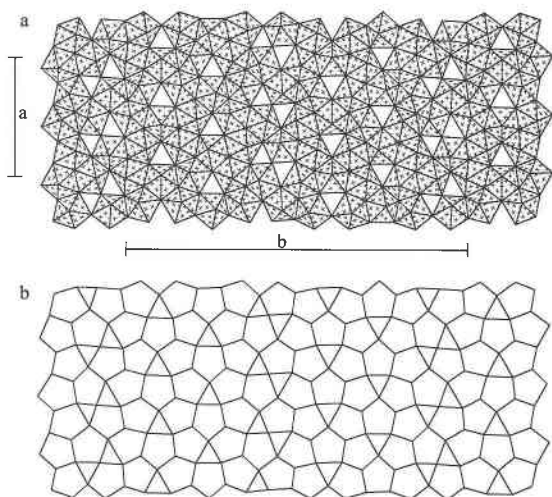
FIGURE 2. The sheet of U polyhedra in the structure of van-dendriesscheite. The projection is along [001]. (a) Polyhedral representation, (b) sheet anion topology derived by the method of Burns et al. (1996). U polyhedra are shaded with crosses.



FIGURE 3. The D, U, and P chains that can be used to de-scribe sheet anion topologies (Miller et al. 1996).

scribed using two distinct chains of polygons; these are shown in Figure 3. The U and D chains are composed of alternating triangles and pentagons and differ only in their orientation (Miller et al. 1996). The P chain contains only pentagons that share edges (Miller et al. 1996). In the vandendriesscheite anion topology, the chains extend along [100]. In the [010] direction, the anion topology contains U, D, and P chains in the sequence PDUPUP-UPUDPDPDPDUPUPU. . . .

## Hydrogen bonding

As is usually the case for uranyl phases, it was not possible to determine the positions of the H atoms directly from the X-ray diffraction data. However, most aspects of the hydrogen bonding can be established on the basis of crystal-chemical arguments.

Eleven symmetrically distinct $OH^-$ groups are bonded to U within the sheets. Owing to the repulsion between the $U^{6+}$ and $H^+$ cations, it is reasonable to expect the $OH^-$ groups to donate hydrogen bonds to $H_2O$ groups in the interlayer, rather than to anions within the sheet of uranyl polyhedra. On the basis of anion-anion separations and U-O-hydrogen bond angles, there is only one possible hydrogen-bond acceptor for each $OH^-$ group. In each case the unambiguous choice of acceptor is an $H_2O$ group located in the interlayer; the possible hydrogen bonds are listed in Table 7.

Two structurally different types of $H_2O$ groups are present in the structure: those that bond to Pb and those that are held in position by hydrogen bonding only. It is common for $H_2O$ to be tetrahedrally coordinated in structures (Hawthorne 1992); thus, the $H_2O$ groups that bond to Pb may accept a hydrogen bond as well as donating two hydrogen bonds. Typically, the $H_2O$ groups that are held in the structure only by hydrogen bonding will ac-
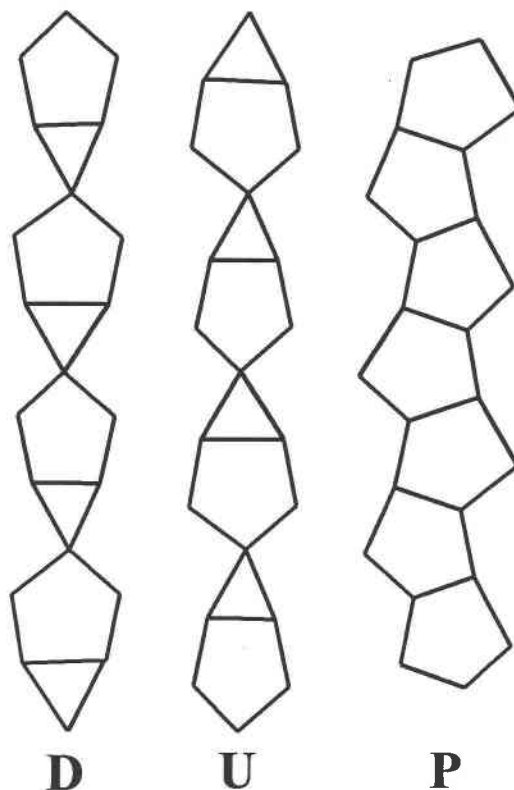
TABLE 7. Anion-anion separations (Å) and angles at $H_2O$ groups (°) corresponding to proposed hydrogen bonding in vandendriesscheite

| | | | | | |
|---|---|---|---|---|---|
| OH2-H₂O42 | 3.04(5) | | H₂O41-O21g | 2.72(7) | 86(2) |
| OH4-H₂O40 | 2.60(5) | | H₂O41-O29h | 2.91(7) | |
| OH6-H₂O45a | 2.73(5) | | H₂O42-O5 | 2.78(5) | 123(1) |
| OH8-H₂O38 | 2.80(5) | | H₂O42-O3li | 3.16(5) | |
| OH12-H₂O43a | 2.98(5) | | H₂O43-O33i | 2.94(4) | 72(1) |
| OH15-H₂O47 | 2.99(5) | | H₂O43-H₂O39h | 2.96(5) | |
| OH17-H₂O39b | 2.62(4) | | H₂O44-O21 | 3.03(5) | 90(1) |
| OH18-H₂O38c | 2.85(5) | | H₂O44-H₂O42j | 2.86(5) | |
| OH19-H₂O44d | 2.86(5) | | H₂O45-O35f | 2.92(6) | 132(2) |
| OH22-H₂O48a | 2.55(5) | | H₂O45-H₂O46k | 3.01(9) | |
| OH27-H₂O42d | 3.14(5) | | H₂O46-O11 | 3.01(9) | 100(3) |
| | | | H₂O46-O13b | 2.80(9) | |
| H₂O38-H₂O40 | 2.96(6) | 80(1) | H₂O47-O34h | 2.99(5) | 66(1) |
| H₂O38-H₂O45 | 2.95(6) | | H₂O47-H₂O43 | 2.66(5) | |
| H₂O39-O9c | 2.97(5) | 84(1) | H₂O48-O23m | 2.99(5) | 77(1) |
| H₂O39-O36d | 2.85(4) | | H₂O48-O32l | 3.00(6) | |
| H₂O40-O16e | 3.00(5) | 91(1) | | | |
| H₂O40-O35f | 2.93(5) | | | | |

Note: a = $x + ½$, $y$, $-z + 1½$; b = $-x + 2$, $y - ½$, $-z + 1½$; c = $x + ½$, $-y + ½$, $-z + 2$; d = $x$, $-y + ½$, $z + ½$; e = $x - ½$, $-y + ½$, $-z + 2$; f = $x - 1$, $-y + ½$, $z + ½$; g = $x - ½$, $-y + ½$, $-z + 1$; h = $x - ½$, $y$, $-z + 1½$; i = $x$, $-y + ½$, $z - ½$; j = $x + ½$, $-y + ½$, $-z + 1$; k = $-x + 1$, $-y$, $-z + 2$; l = $-x + 1½$, $-y$, $z + ½$; m = $-x + 1½$, $y - ½$, $z$.
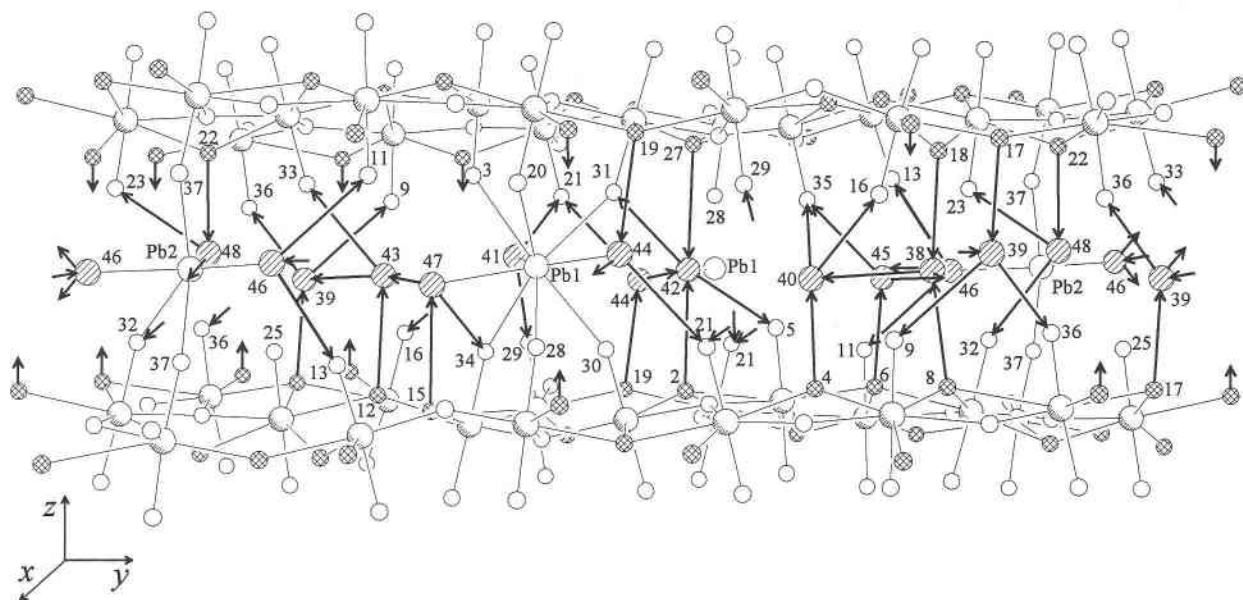
**FIGURE 4.** The interlayer constituents in the structure of vandendriesscheite. Probable hydrogen bonds are shown as solid arrows, with the tail of the arrow at the donor and the arrowhead at the acceptor of the hydrogen bond. The atoms are shown as follows: U = circles shaded in lower left only; Pb = unshaded large circles; O = unshaded small circles; OH⁻ = cross-hatched circles; H₂O = circles shaded with parallel lines.

cept two hydrogen bonds, as well as donating two hydrogen bonds, resulting in a tetrahedral coordination about the central O atom.

The bond-valence sums at the anion positions (Table 6), which exclude contributions from hydrogen atoms, help to identify likely acceptors of hydrogen bonds. Six different O atoms bond to three U atoms and the bond-valence sums range from 1.96 to 2.09 v.u., indicating that none of these are likely acceptors of a hydrogen bond. The bond-valence sums at the OH⁻ positions range from 1.12 to 1.38 v.u.; assuming the O-H donor bond of the OH⁻ group has a bond valence of ~0.8 v.u., the OH⁻ groups are not likely to accept hydrogen bonds. The $O_{Ur}$ anions have bond-valence sums ranging from 1.47 to 1.92 v.u., indicating that many must accept one, or in some cases two, hydrogen bonds. Finally, those H₂O groups that bond to Pb should accept a single hydrogen bond or no hydrogen bond, whereas the remaining H₂O groups probably accept two hydrogen bonds to satisfy their bond-valence requirements.

Anion-anion separations in the range 2.5 to 3.1 Å indicate possible hydrogen bonds, with smaller separations implying stronger hydrogen bonding. However, for hydrogen bonds to occur, the donor and acceptor anions should not both be part of the same Pb polyhedron, as this involves repulsion between the H⁺ and Pb²⁺ cations. Another useful indicator of possible hydrogen bonds is the relationship of accepted and donated bonds, which should be in an approximately tetrahedral arrangement.

Each of the above-mentioned aspects of the hydrogen bonding has been used to develop a crystal-chemically feasible hydrogen bonding system for the structure of

vandendriesscheite. The proposed hydrogen bonds are illustrated in Figure 4 and listed in Table 7. The hydrogen bonds provide a substantial amount of linkage from the sheets of uranyl polyhedra to the interlayer constituents. Each OH⁻ group in the sheets donates its hydrogen bond to an interlayer H₂O group, whereas hydrogen bonds that are donated from interlayer H₂O groups to the sheets are accepted by $O_{Ur}$ atoms. Consider first those H₂O groups that are bonded to Pb cations. These are the H₂O41, H₂O44, H₂O46, H₂O47, and H₂O48 anions. The H₂O41 anion donates a hydrogen bond to both adjacent sheets, but it does not accept a hydrogen bond. Both the H₂O44 and H₂O47 anions donate one hydrogen bond to a sheet, but the remaining hydrogen bond is accepted by an interlayer H₂O group. However, the H₂O44 and H₂O47 anions link to the other adjacent sheet by accepting hydrogen bonds donated by OH⁻ groups contained within the sheet. The H₂O46 and H₂O48 anions donate hydrogen bonds to both adjacent sheets and accept a single hydrogen bond from an interlayer H₂O group.

Next consider the H₂O groups that are held in the structure only by hydrogen bonding; these are the H₂O38, H₂O39, H₂O40, H₂O42, H₂O43, and H₂O45 anions. The H₂O38 anion accepts a hydrogen bond from an OH⁻ group of each adjacent sheet, and donates both of its hydrogen bonds to interlayer H₂O groups. The H₂O39 and H₂O40 anions both donate each of their hydrogen bonds to the same sheet, but intersheet linkage is provided because each of these anions also accepts a hydrogen bond from the other adjacent sheet, as well as from an interlayer H₂O group. The H₂O43 and H₂O45 anions both provide intersheet linkage by donating a hydrogen bond to
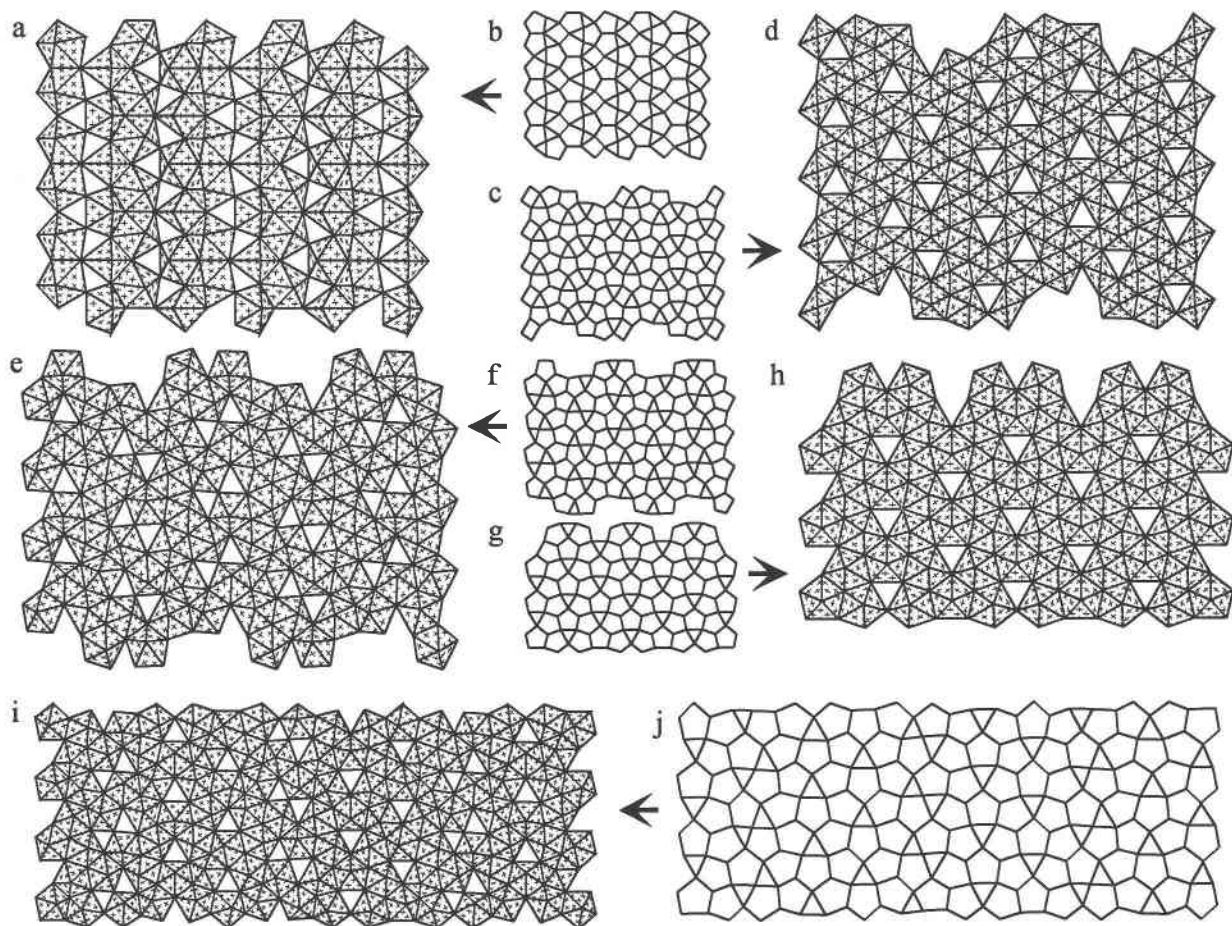
**FIGURE 5.** Polyhedral representations and anion topologies of the sheets that occur in lead uranyl oxide hydrate minerals. (**a**) curite, (**b**) curite anion topology, (**c**) sayrite anion topology, (**d**) sayrite, (**e**) fourmarietite, (**f**) fourmarierite anion topology, (**g**) richetite anion topology, (**h**) richetite, (**i**) vandendriesscheite, (**j**) vandendriesscheite anion topology. The sheet anion topologies were derived using the method of Burns et al. (1996). U polyhedra are shaded with crosses.

an adjacent sheet, as well as by accepting a hydrogen bond from the other adjacent sheet. Both of these anions also donate and accept hydrogen bonds to and from interlayer $H_2O$ groups. Additional intersheet bonding is provided by the $H_2O39$ anion that donates a hydrogen bond to both adjacent sheets, as well as accepting a hydrogen bond from both an $OH^-$ group located in a sheet and an interlayer $H_2O$ group.

## RELATIONSHIPS TO OTHER SPECIES

Although seven lead uranyl oxide hydrate minerals have been described (Finch and Ewing 1992), crystal structures have only been reported for fourmarierite (Piret 1985), sayrite (Piret et al. 1983), curite (Taylor et al. 1981), and vandendriesscheite (this study). In addition, we have recently determined the structure of richetite ($R$ = 9%). Each of these structures contains sheets of uranyl polyhedra with Pb cations and $H_2O$ groups located in interlayer positions.

Each of the known lead uranyl oxide hydrate mineral structures contains a unique sheet of uranyl polyhedra, as shown in Figure 5. The curite (Fig. 5a) and sayrite (Fig. 5d) sheets both contain $Ur\phi_4$ and $Ur\phi_5$ polyhedra, but the arrangement of the polyhedra is significantly different in the two sheets. The curite sheet is not known from another structure but a sheet with the same topological arrangement as the sayrite sheet has been found in the structure of $K_2[(UO_2)_5O_8](UO_2)_2$ (Kovba 1972), which has both K and $U^{6+}$ cations in the interlayer.

The sheets in the structure of fourmarierite (Fig. 5e), richetite (Fig. 5h), and vandendriesscheite (Fig. 5i) contain only $Ur\phi_5$ polyhedra. A sheet with the same topological arrangement as the fourmarierite sheet occurs in the structure of schoepite, $[(UO_2)_8O_2(OH)_{12}](H_2O)_{12}$ (Finch et al. 1996), where the interlayer contains only $H_2O$ groups. Sheets that are topologically identical to the richetite sheet occur in several structures: protasite, $Ba[(UO_2)_3O_3(OH)_2](H_2O)_3$ (Pagoaga et al. 1987); billietite, $Ba[(UO_2)_3O_2(OH)_3](H_2O)_4$ (Pagoaga et al. 1987); becquerelite, $Ca[(UO_2)_3O_2(OH)_3]_2(H_2O)_8$ (Pagoaga et al.

1987); and $\alpha$-$U_3O_8$ (Loopstra 1977). In the structures of protasite and billietite, the interlayer contains Ba cations and $H_2O$ groups, and the interlayer of the becquerelite structure has Ca cations and $H_2O$ groups. There is no interlayer species in $\alpha$-$U_3O_8$; sheets are connected together by sharing anions.

The vandendriesscheite sheet is more complex than those known in other lead uranyl oxide hydrate structures (Fig. 5). It is informative to consider the topological arrangement of the anions in the sheet in detail, as this facilitates the comparison with related structures. The basic anion topology of the vandendriesscheite sheet (Fig. 2b) does not distinguish between $O^{2-}$ and $OH^-$. However, the distribution of $O^{2-}$ and $OH^-$ in the sheet is important because it relates to the valence of the sheet. For example, the structure of schoepite contains a neutral sheet with composition $[(UO_2)_8O_2(OH)_{12}]$, although the topological arrangement of the sheet is identical to that of the fourmarierite sheet, with composition $[(UO_2)_4O_3(OH)_4]^{2-}$. Likewise, the sheet in the structures of becquerelite and billietite has the composition $[(UO_2)O_4(OH)_6]^{2-}$; a topologically identical sheet occurs in the structure of protasite, but the sheet has the composition $[(UO_2)_3O_3(OH)_2]^{2-}$.

The anion topologies of the sheets in the structures of vandendriesscheite, schoepite, and becquerelite are provided in Figure 6, with the location of $OH^-$ groups given by circles in each anion topology. Figure 6 demonstrates that the vandendriesscheite anion topology is structurally intermediate between the schoepite and becquerelite anion topologies. Specifically, infinite slabs taken from the schoepite and fourmarierite anion topologies can be used to construct the vandendriesscheite anion topology (Fig. 6). Thus, the vandendriesscheite sheet is structurally intermediate between the schoepite and becquerelite sheets, as the sheets of polyhedra are obtained from the anion topology simply by populating each pentagon with a $(UO_2)^{2+}$ uranyl ion.

## PARAGENESIS OF LEAD URANYL OXIDE HYDRATES

Uraninite, $UO_{2+x}$, is the most common mineral in U ore deposits. Uraninite is isostructural with fluorite, and most of the U is present as $U^{4+}$. The uraninite in Precambrian U deposits contains substantial amounts of radiogenic Pb. Uraninite is unstable under highly oxidizing conditions and decomposes, releasing both the U (as $U^{6+}$) and the Pb into the environment, giving cause for concern where U mine tailings interact with the environment. Under arid conditions, uranyl oxide hydrates are precipitated locally, usually in contact with the decomposing uraninite (Finch and Ewing 1992). The onset of alteration of uraninite involves the precipitation of schoepite, which contains no Pb, and vandendriesscheite, which contains the least Pb of any of the lead uranyl oxide hydrates. The $U^{6+}$ ion, which is present as a $(UO_2)^{2+}$ uranyl ion in oxidizing fluids, is much more mobile than the $Pb^{2+}$ cation (Mann and Deutscher 1980). Therefore, continued interaction of the minerals with an oxidizing fluid preferentially removes $U^{6+}$, thus the paragenetic sequence of lead



Schoepite Anion-Topology

Becquerelite Anion-Topology

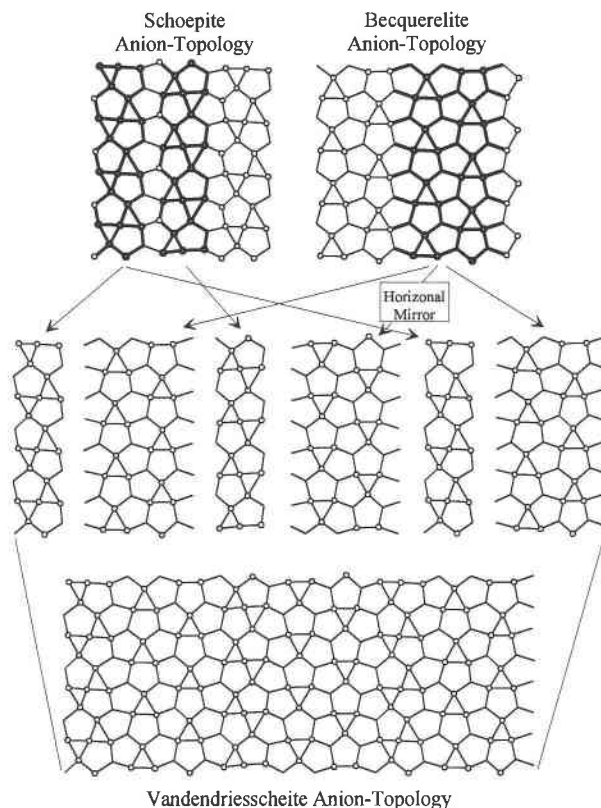Horizonal Mirror

Vandendriesscheite Anion-Topology

**FIGURE 6.** A demonstration of how infinite slabs of the schoepite and becquerelite sheet anion topologies may be used to construct the vandendriesscheite sheet anion topology. The locations of $OH^-$ groups are indicated by circles.

uranyl oxide hydrates involves an increase of the Pb:U ratios with increasing alteration (Frondel 1958; Finch and Ewing 1992; Finch 1994).

The structure of schoepite has neutral sheets and only $H_2O$ groups in the interlayer (Finch et al. 1996). Incorporation of $Pb^{2+}$ into interlayer positions in the structure of a uranyl oxide hydrate requires that the sheets of uranyl polyhedra are negatively charged, as the only other interlayer species is neutral $H_2O$. Thus, the Pb:U ratio is constrained by the charge of the sheet, which is conveniently given as the ratio of U atoms to negative charge. The five lead uranyl oxide hydrate minerals with known structures are arranged according to increasing sheet charge in Table 8. Masuyite is a lead uranyl oxide hydrate, although the structure has not been resolved. Finch and Ewing (1992) reported that crystals of masuyite show a range of compositions and may actually correspond to multiple phases. On the basis of electron microprobe analyses, Finch and Ewing (1992) reported that "masuyite I" has the formula $PbU_3O_{10}\cdot3-4H_2O$. A recent study of a large sampling of masuyite crystals from the Shinkolobwe deposit (Congo) has shown that two distinct minerals are represented, one with the formula $PbU_3O_{10}\cdot4H_2O$, which is identical to "masuyite I" of Finch and Ewing (1992), and the other with the formula

**TABLE 8.** Summary of the chemistries of lead uranyl oxide hydrates

| Name | U:charge | Pb:U | Sheet composition | Ref. |
|---|---|---|---|---|
| Sayrite | 1:0.80 | 1:2.5 | $[(UO_2)_5O_6(OH)_2]$ | 1 |
| Curite | 1:0.75 | 1:2.67 | $[(UO_2)_8O_8(OH)_6]$ | 2 |
| Fourmarierite | 1:0.50 | 1:4.0 | $[(UO_2)_4O_3(OH)_4]$ | 3 |
| Richetite | 1:0.47 | 1:4.15 | | 4 |
| Vandendriesscheite | 1:0.30 | 1:6.36 | $[(UO_2)_{10}O_6(OH)_{11}]$ | 5 |
| Schoepite | neutral | no Pb | $[(UO_2)_8O_2(OH)_{12}]$ | 6 |

*Note:* 1 = Piret et al. (1983); 2 = Taylor et al. (1981); 3 = Piret (1985); 4 = Burns et al. (in preparation); 5 = this study; 6 = Finch et al. (1996).

$Pb_4U_9O_{31}\cdot10H_2O$ (Deliens and Piret 1996). "Masuyite I" is the Pb analogue of protasite, consistent with the prediction of Pagoaga (1983) that the structure of masuyite is based on the same sheet of uranyl polyhedra as the structure of protasite. Thus, the sequence of lead uranyl oxide hydrate minerals in order of increasing Pb content is: schoepite (no Pb) → vandendriesscheite → richetite → fourmarierite → "masuyite I" → curite → sayrite (modified from Finch and Ewing 1992). The mineral with composition $Pb_4U_9O_{31}\cdot10H_2O$ reported by Deliens and Piret (1996) has a Pb:U ratio of 1:1.25, making it even more Pb rich than sayrite.

The vandendriesscheite sheet is structurally intermediate between the schoepite and becquerelite sheets (Fig. 6). The sheets in the structures of becquerelite and protasite have the same topological arrangements (Pagoaga et al. 1987) but different distributions of $O^{2-}$ and $OH^-$, resulting in different U-to-charge ratios for the sheets. The structure of richetite also contains sheets that are topologically identical to the becquerelite and protasite sheets, but the U-to-charge ratio is intermediate between the becquerelite and protasite sheets. Thus, the richetite sheet is structurally intermediate between the becquerelite and protasite sheets. The Pb analogue of becquerelite is not known, but there is no apparent reason why it should not occur. Assuming that "masuyite I" is isostructural with protasite, there is a continuous sequence of crystal structures that involves a systematic modification of the sheets of U polyhedra that corresponds to increasing sheet charge and increasing Pb content: schoepite (Pb:U = 0, U:valence = 0) → vandendriesscheite (1:6.36, 1:0.30) → Pb-becquerelite (1:6.0, 1:0.33) → richetite (1:4.14, 1:0.47) → "masuyite I" (1:3.0, 1:0.66). This sequence of structures is identical to the paragenetic sequence for the lead uranyl oxide hydrate minerals.

## RELEVANCE TO NUCLEAR WASTE DISPOSAL

Young spent nuclear fuel does not contain significant amounts of radiogenic Pb, thus lead uranyl oxide hydrate phases do not form when spent fuel is oxidized. However, the interaction of $UO_2$ and spent fuel with groundwater similar in composition to that found at Yucca Mountain results in the formation of various uranyl oxide hydrates, including schoepite, dehydrated schoepite, becquerelite, and the Na analogue of compreignacite, $Na_2[(UO_2)_3O_2-$

$(OH)_3]_2(H_2O)_8$, as well as uranyl silicates such as soddyite, $(UO_2)_2(SiO_4)(H_2O)_2$, sodium boltwoodite, $(Na,K)(H_3O)[(UO_2)(SiO_4)]$, and uranophane, $Ca[(UO_2)(SiO_3-OH)]_2(H_2O)_5$ (Wronkiewicz et al. 1992, 1996; Finn et al. 1996). The observed paragenetic sequence when $UO_2$ or spent fuel is corroded under oxidizing conditions is identical to that found in weathered uraninite deposits. Specifically, the sequence is uraninite → schoepite → alkali and alkaline earth uranyl oxide hydrates → uranyl silicates (Wronkiewicz et al. 1992, 1996).

During the burn-up of nuclear fuel, as much as 4% of the U in the fuel will undergo fission to produce stable and radioactive fission products (e.g., Sr, Cs, I, Tc). In addition, transuranic elements (e.g., Np, Pu, Am, Cm) are formed from U by neutron capture. The radionuclide inventory contained in the spent fuel is a cause for environmental concern, since much of it may be released to the environment during the oxidative dissolution of the fuel matrix. However, recent leaching tests performed on spent fuel under oxidizing conditions indicate that some of the radionuclides released from the spent fuel are incorporated into the products of alteration, which are mainly uranyl phases. It is possible that radionuclides such as $^{137}Cs$ and $^{90}Sr$ are incorporated into the interlayer positions of uranyl oxide hydrate phases that form as alteration products. This possibility is supported by the observation that both of these radionuclides are in part retained on the fuel sample during leaching experiments on spent fuel (Finn et al. 1996).

The current study has demonstrated a clear relationship between the paragenetic sequence of lead uranyl oxide hydrate minerals and their crystal structures. The occurrence of the vandendriesscheite and richetite sheets is significant, from the point of view of spent fuel alteration, because changes in the topology and anion distribution of the sheets of uranyl polyhedra can occur to accommodate various interlayer constituents, such as radioactive fission products. The discovery of the vandendriesscheite sheet, which contains components of both the schoepite and becquerelite sheets, and the richetite sheet, which is intermediate between the becquerelite and protasite sheets, strongly suggests that these sheets are involved in the transformation of early formed schoepite to the alkaline earth uranyl oxide hydrates that form later during the oxidative dissolution of spent fuel.

## REFERENCES CITED

Brese, N.E. and O'Keeffe, M. (1991) Bond-valence parameters for solids. Acta Crystallographica, B47, 192–197.
Burns, P.C., Miller, M.L., and Ewing, R.C. (1996) $U^{6+}$ minerals and inorganic phases: a comparison and hierarchy of crystal structures. Canadian Mineralogist, 34, 845–880.
Burns, P.C., Hawthorne, F.C., and Ewing, R.C. (1997) The crystal chem-

istry of hexavalent uranium: Polyhedral geometries, bond-valence parameters, and polyhedral polymerization. Canadian Mineralogist (in press).

Christ, C.L. and Clark, J.R. (1960) Crystal chemical studies of some uranyl oxide hydrates. American Mineralogist, 45, 1026–1061.

Cromer, D.T. and Liberman, D. (1970) Relativistic calculations of anomalous scattering factors for X rays. Journal of Chemical Physics, 53, 1891–1898.

Cromer, D.T. and Mann, J.B. (1968) X-ray scattering factors computed from numerical Hartree-Fock wave functions. Acta Crystallographica, A24, 321–324.

Deliens, M. and Piret, P. (1996) Les masuyites de Shinkolobwe (Shaba, Zaire) constituent un groupe forme de deux variétes distinctes par leur composition chimique et leurs propriétes radiocristallographiques. Bulletin de l'Institut Royal des Sciences Naturelles de Belgique, Sciences de la Terre, 66, 187–192.

Evans, H.T., Jr. (1963) Uranyl ion coordination. Science, 141, 154–157.

Ewing, R.C. (1993) The long-term performance of nuclear waste forms: natural materials-three case studies. In C.G. Interante and R.T. Pabalan, Eds., Scientific Basis for Nuclear Waste Management XVI, P. 559–568. Materials Research Society Proceedings,

Finch, R.J. (1994) Paragenesis and crystal chemistry of the uranyl oxide hydrates. Ph.D. Thesis, University of New Mexico, Albuquerque, NM.

Finch, R.J. and Ewing, R.C. (1992) The corrosion of uraninite under oxidizing conditions. Journal of Nuclear Materials, 190, 133–156.

Finch, R.J., Cooper, M.A., and Hawthorne, F.C. (1996) The crystal structure of schoepite, $[(UO_2)_8O_2(OH)_{12}](H_2O)_{12}$. Canadian Mineralogist, 34, 1071–1088.

Finn, P.A., Hoh, J.C., Wolf, S.F., Slater, S.A., and Bates, J.K. (1996) The release of uranium, plutonium, cesium, strontium, technetium and iodine from spent fuel under unsaturated conditions. Radiochimica Acta, 74, 65–71.

Forsyth, R.S. and Werme, L.O. (1992) Spent fuel corrosion and dissolution. Journal of Nuclear Materials, 190, 3–19.

Frondel, C. (1958) Systematic mineralogy of uranium and thorium. U.S. Geological Survey Bulletin, 1064.

Hawthorne, F.C. (1992) The role of OH and $H_2O$ in oxide and oxysalt minerals. Zeitschrift für Kristallographie, 201, 183–206.

Johnson, L.H. and Werme, L.O. (1994) Materials characteristics and dissolution behavior of spent nuclear fuel. Material Research Society Bulletin, 24–27.

Kovba, L.M. (1972) Crystal structure of $K_2U_7O_{22}$. Journal of Structural Chemistry, 13, 235–238.

Loopstra, B.O. (1977) On the structure of $\alpha$-$U_3O_8$. Journal of Inorganic and Nuclear Chemistry, B26, 656–657.

Mann, A.W. and Deutscher, R.L. (1980) Solution chemistry of lead and zinc in water containing carbonate, sulphate and chloride ions. Chemical Geology, 29, 293–311.

Miller, M.L., Finch, R.J., Burns, P.C., and Ewing, R.C. (1996) Description and classification of uranium oxide hydrate sheet anion topologies. Journal of Materials Research, 11, 3048–3056.

Pagoaga, M.K. (1983) The crystal chemistry of the uranyl oxide hydrate minerals. Ph.D. Thesis, University of Maryland.

Pagoaga, M.K., Appleman, D.E., and Stewart, J.M. (1987) Crystal structures and crystal chemistry of the uranyl oxide hydrates becquerelite, billietite, and protasite. American Mineralogist, 72, 1230–1238.

Pearcy, E.C., Prikryl, J.D., Murphy, W.M., and Leslie, B.W. (1994) Alteration of uraninite from the Nopal I deposit, Peña Blanca District, Chihuahua, Mexico, compared to degradation of spent nuclear fuel in the proposed U.S. high-level nuclear waste repository at Yucca Mountain, Nevada. Applied Geochemistry, 9, 713–732.

Piret, P. (1985) Structure cristalline de la fourmariérite, $Pb(UO_2)_4O_3$-$(OH)_4.4H_2O$. Bulletin de Minéralogie, 108, 659–665.

Piret, P., Deliens, M., Piret-Meunier, J., and Germain, G. (1983) La sayrite, $Pb_2[(UO_2)_5O_6(OH)_2].4H_2O$, nouveau minéral; propriétés et structure cristalline. Bulletin de Minéralogie, 106, 299–304.

Protas, J. (1959) Contribution á l'étude des oxides d'uranium hydratés. Bulletin de la Société Francaise de Minéralogie et de la Cristallographie, 82, 239–272.

Taylor, J.C., Stuart, W.L., and Mumme, I.A. (1981) The crystal structure of curite. Journal of Inorganic and Nuclear Chemistry, 43, 2419–2423.

Vaes, J.F. (1947) Six nouveaux minéraux d'urane provenant de Shinkolobwe (Katanga). Annales Sociéte Géologique Belgique, 70, B212–B229.

Wadsten, T. (1977) The oxidation of polycrystalline uranium dioxide in air at room temperature. Journal of Nuclear Materials, 64, 315.

Wang, R. and Katayama, Y.B. (1982) Dissolution mechanisms for $UO_2$ and spent fuel. Nuclear and Chemical Waste Management, 3, 83–90.

Wronkiewicz, D.J., Bates, J.K., Gerding, T.J., Veleckis, E., and Tani, B.S. (1992) Uranium release and secondary phase formation during unsaturated testing of $UO_2$ at 90°C. Journal of Nuclear Materials, 190, 107–127.

Wronkiewicz, D.J., Bates, J.K., Wolf, S.F., and Buck, E.C. (1996) Ten-year results from unsaturated drip tests with $UO_2$ at 90°C: implications for the corrosion of spent nuclear fuel. Journal of Nuclear Materials, 238, 78–95.